Materials Advances

PAPER

Check for updates

A naphthalene–phenanthro[9,10-*d*]imidazole-based π-conjugated molecule with a self-assembly-induced tuneable multiple fluorescence output exhibits artificial light-harvesting properties†

Priya Rana,‡[a] Mallayasamy Siva,‡[a] Rabindranath Lo*[b] and Priyadip Das [ID] *[a]

Among promising new materials, π-conjugated organic molecules are considered an attractive platform for the design and development of a wide range of self-assembled superstructures with desirable optical and electrical properties necessary for use in organic optoelectronics applications. The optical and electrical properties of π-conjugated organic molecules and their possible applications are usually determined by their primary molecular structure and their intermolecular interactions in the self-assembled state. However, satisfying the structural requirements for achieving tuneable optical properties is a difficult task, which makes the design and development of novel high-performance π-conjugated organic systems for nano-optoelectronics a considerable challenge. In this paper, we report on the design and synthesis of a naphthalene–phenanthro[9,10-*d*] imidazole-based π-conjugated Schiff base molecule (**L1**) that exhibits aggregation-induced tunable luminescence properties facilitated by solvent polarity. Upon varying the medium polarity of the self-assembly medium, **L1** self-assembles into various superstructures with distinct morphologies and generates multiple tunable emission colours (blue–green–yellow–white). In a highly polar THF : water = 1 : 9 medium, it displays aggregation-induced white light emission. These single component-based white-light emitters attract broad attention due to their potential applications in lighting devices and display media. Computational studies incorporating full geometry optimization, time-dependent density functional theory (TDDFT) calculations and molecular dynamics (MD) simulations were utilized to elucidate the enhanced π–π interaction influenced by increasing solvent polarity and orbitals involved in electronic transitions associated with different self-assembled states. More importantly, we constructed a highly efficient artificial light-harvesting system in a THF : water = 1 : 1 medium based on self-assembled **L1** and rhodamine B (RhB), where **L1** acts as an energy donor and RhB acts as an acceptor, exhibiting a strong antenna effect at a substantial donor/acceptor ratio. Our findings provide a novel versatile approach for developing efficient light-harvesting systems based on the supramolecular self-assembly of suitably designed π-conjugated organic molecules with tuneable multiple emission properties.

[a] Department of Chemistry, SRM Institute of Science and Technology, SRM Nagar, Potheri, Kattankulathur, Tamil Nadu-603203, India. E-mail: priyadipcsmcri@gmail.com, priyadip@srmist.edu.in
[b] Institute of Organic Chemistry and Biochemistry, Czech Academy of Sciences, Flemingovo náměstí 542/2, Prague 160 00, Czech Republic. E-mail: rabindranath.lo@uochb.cas.cz

† Electronic supplementary information (ESI) available: UV spectra, emission spectra, length and width distribution graph, fluorescence colour photographs, minima structure of dimers, and bond length variations in monomers. See DOI: https://doi.org/10.1039/d4ma00806e
‡ Equal contribution

Introduction

The primary energy source for living organisms is photosynthesis, a process utilized by green plants, algae and certain bacteria to convert solar energy into chemical energy.[1,2] In the first stage of photosynthesis, light is employed to generate high-energy molecules. The energy harvested in this stage is stored inside the cell in the form of adenosine triphosphate (ATP) and then converted into chemical energy.[3] Inspired by this, researchers have mimicked this natural process and developed various artificial light-harvesting systems (LHSs).[4] These systems exhibit light-harvesting properties mediated by

Förster resonance energy transfer (FRET).[5–8] There are two essential preconditions for this process to take place: First, the donor should be densely packed without any considerable self-quenching effect, and secondly, the donor/acceptor ratio should be sufficiently high. When these preconditions are met, excitation energy can be transferred with minimum energy loss. In the FRET process, energy is usually transferred between a donor and an acceptor through covalent bonds or non-covalent interactions. Among the LHSs being developed, those based on non-covalent interactions are particularly intriguing due to their ease of synthesis, tuneable optical properties, energy transfer efficiency and solution processability, which offer several possibilities for the utilization of solar light in different fields. With the aim of developing clean and sustainable energy technologies, several artificial LHSs have been developed.[9–12] Among them, self-assembled supramolecular systems have received substantial attention not only due to their tuneable and functional molecular structure, but also because effective energy transfer between chlorophyll and protein in natural systems also depends on supramolecular self-assembly.[4,13–16] For example, Yang *et al.* reported an extremely effective self-assembled organic nanocrystal-based light-harvesting system able to mimic chlorosomes.[17] However, detailed investigations of these artificial LHSs provide insights into fundamental processes and help to explore exciting applications in photovoltaics, photocatalysis and photopolymerization.[5,6,11,18–21] The appropriate choice of a supramolecular scaffold, which can be a dendrimer, polymer or metal–organic framework, which can avoid fluorescence quenching with a corresponding FRET pair, is essential for achieving a promising light-harvesting system.[22–27] Prof. Stang and his co-workers have developed a highly efficient light-harvesting system based on self-assembled fluorescent Pt(II) metallacycles.[6] Recently, small organic functional π-conjugated molecules have received considerable interest due to their ability to self-assemble,[28,29] their tuneable optical behaviour[30,31] and their favourable charge transfer properties. These characteristics improve the efficiency of solar cells and provide promising advancements in organic photovoltaic and light-emitting diode technologies.[32–34]
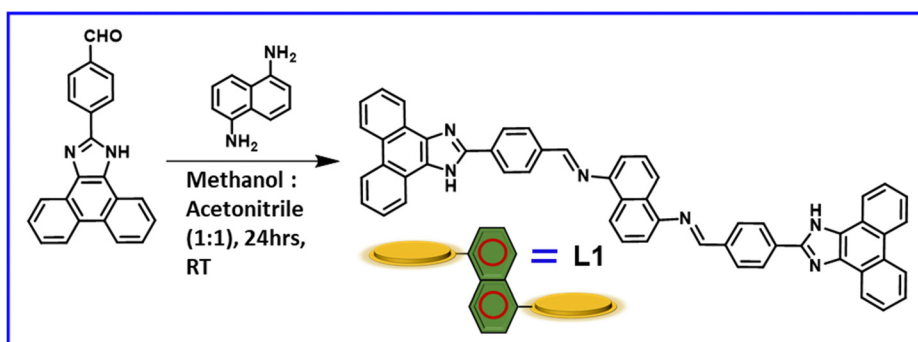
The unique and varied functionalities of self-assembled π-conjugated molecules are promising for applications in molecular switches, photo-controllable smart materials, and photo-patterning.[35–37] In this context, Chai *et al.* have developed a series of π-conjugated multifunctional molecules. Upon exposure to UV irradiation, one of them exhibits aggregation-induced emission (AIE) in an aqueous medium, associated with a reversible change in emission colour, and forms an effective light-harvesting system with rhodamine B.[38] Herein we report on the design and synthesis of the naphthalene–phenanthro[9,10-*d*]-imidazole-based π-conjugated organic Schiff base compound named **L1**. We synthesized this probe *via* a condensation reaction of naphthalene-1,5-diamine with a π-conjugated aldehyde ligand, 4-(1*H*-phenanthro[9,10-*d*]-imidazole-2-yl) benzaldehyde (A1). We then investigated the solvent polarity-induced optical properties and the aggregation behaviour of this newly synthesized optical probe. Our results show that **L1** exhibits tuneable emission properties that are induced by aggregation facilitated by favourable solvent polarity, which helps to understand the self-assembly of **L1** into different superstructures varying in morphology depending on the polarity of the medium. Furthermore, we have successfully employed the self-assembled superstructures generated from **L1** in a THF:water = 1:1 mixture to develop a highly effectual LHSs utilizing the commercial fluorophore rhodamine B (RhB). In this system, aggregated forms of **L1** serve as donors whereas rhodamine B functions as an acceptor. Overall, our results clearly reflect the potentiality of using self-assembled **L1** in sensing, bioimaging and the development of optoelectronic devices.

Results and discussion

Synthesis

We synthesized the π-conjugated Schiff base molecule **L1** *via* a straightforward coupling reaction between naphthalene-1,5-diamine with a π-conjugated aldehyde ligand, 4-(1*H*-phenanthro[9,10-*d*]-imidazole-2-yl)-benzaldehyde (A1), in a methanol:acetonitrile mixture (1:1) at room temperature (RT), as illustrated in Scheme 1. Details of the synthesis procedure are provided in Scheme S1 and S2 in the Experimental section of the ESI.† We then characterized all the synthesized products using standard analytical techniques (Fig. S1–S3, ESI†).

Scheme 1 Schematic representation of the synthesis of **L1**.

Spectral analysis

We examined whether and how changes in solvent polarity affect the optical properties of **L1**. To this end, we first recorded the UV-Vis absorption spectra of **L1** (20 μM) in a THF:water mixture with the percentage of water ranging from 0% to 90% (v/v). The absorption spectra of **L1** (20 μM) in a pure THF medium exhibited an absorption peak at 378 nm (ε = 3.8 × 10^4 M^{-1} cm^{-1}) and a broad band with an absorption maximum at 476 nm (ε = 2.3 × 10^3 M^{-1} cm^{-1}). The higher energy absorption band at 382 nm is attributed to the intramolecular $\pi–\pi^*$ charge transfer (ICT) transition whereas the broad band absorption maximum at 476 nm is presumably due to the intramolecular charge transfer (CT) transition (Fig. 1A). Upon a gradual increase in the percentage of water (from 0% to 90%) in the THF:water mixture, we observed a noticeable bathochromic shift of the absorption maximum at 382 nm with reduced intensity. In a THF : water = 1 : 9 mixture, the absorption maximum shifted to 394 nm with an eventual distinctive red shift of 16 nm. This kind of bathochromic shift of the CT absorption band can be anticipated for J-type aggregation.[30] Furthermore, for a better understanding of the polarity-induced aggregation process, we recorded the steady-state emission spectra of **L1** in a THF:water mixture of varying polarity by altering the percentage of water from 0 to 90%. In pure THF, the steady-state photoluminescence spectra of **L1** (20 μM) exhibited emission maxima at 533 nm that were observed upon excitation at 382 nm (Fig. 1B). Upon varying the water content in the THF:water mixture, we observed a significant change in the emission spectral pattern of **L1**. As we increased the polarity of the medium from 0 to 50% (THF : water = 1 : 1), the emission maxima underwent a significant bathochromic shift with enhanced emission intensity (Fig. 1B). A further increase in

medium polarity (THF : water = 4 : 6 to 1 : 9) effectively decreased the emission intensity with red-shifted emission maxima and eventually caused a distinctive red shift of the emission maximum by ~72 nm (Fig. 1B).

It is obvious that an increase in medium polarity modifies the non-covalent intermolecular interactions responsible for molecular aggregation. This alters the pattern of molecular assembly, which determines the emissive properties corresponding to particular aggregated states.[39,40] The emission spectral analysis of **L1** exhibited a gradual red shift of the emission maximum with elevated emission intensity as the concentration of water in the THF:water mixture increased from 0 to 50%. This was mainly due to the aggregation-induced emission (AIE) mechanism.[14,30,41] However, upon a further increase in water content in the THF:water mixture (60% to 90%), there was a considerable drop in emission intensity with a steady redshift of the emission maximum, indicating that the aggregation-caused quenching (ACQ) process took place.[42,43] This noticeable steady red shift of the emission maximum with increasing medium polarity confirmed that the J-aggregation pattern of **L1** changed with increasing medium polarity.[39,40] The head-to-tail molecular arrangement due to J-type aggregation enhances the intermolecular electronic communications resulting in strong excitonic coupling and delocalization of the excited states across the molecules. This type of aggregation influences the electronic properties of the aggregates, specifically reduces the energy gap associated with the absorption and emission process with increasing intermolecular noncovalent interaction including $\pi–\pi$ interactions and leads to a significant redshift of the corresponding absorption and emission maxima.[44–47] This red shift of the ICT-based emission maximum with increasing medium polarity is due to the stabilization of the lowest
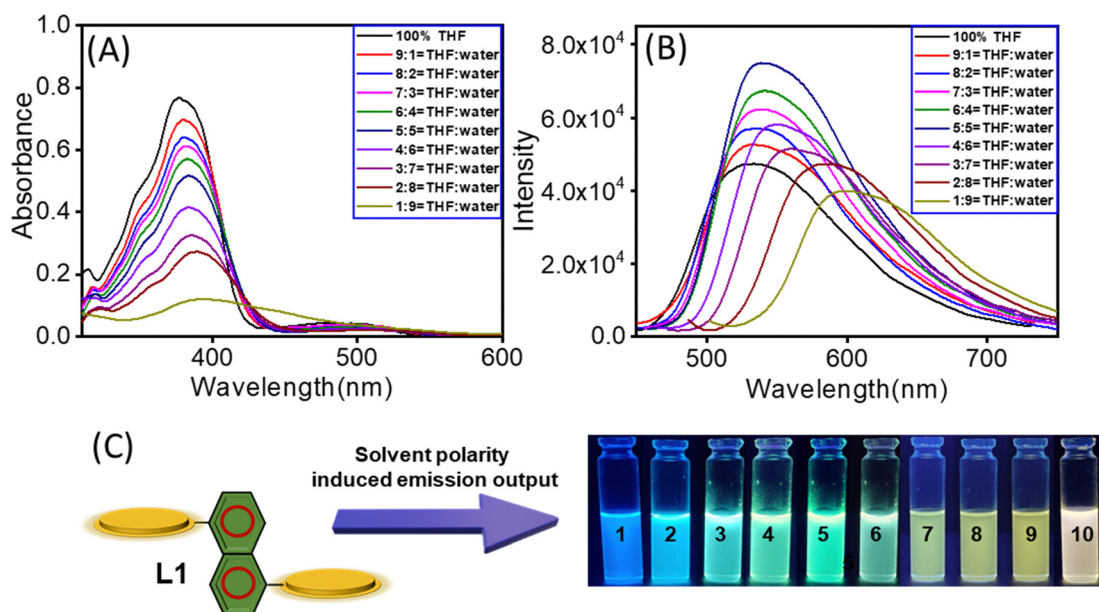

Fig. 1 (A) UV-Vis and (B) emission spectra of **L1** in THF and different THF:water mixtures. (C) Photographs showing the change in fluorescence colours of **L1** upon irradiation with 365 nm light at different ratios of the THF:water mixtures.

unoccupied molecular orbital (LUMO) in the polar medium, which effectively reduces the energy gap associated with that CT transition.[44] Additionally, we investigated the visually detectable luminescence colours generated by **L1** in various THF:water mixtures with varying percentages of water. We observed that the emission colour changed remarkably from blue to green, then to yellow, and finally to white upon varying the water percentage from 0 to 90% in our THF:water mixture (Fig. 1C). The fluorescence spectra obtained for the THF:water = 1:9 mixture almost covered the entire visible region and exhibited white light emission. The above results indicate that the different aggregated states of this π-conjugated system based on **L1** in different THF:water mixed solvent media varying in polarity account for the multiple luminescence colours observed.[31] **L1** can adopt different molecular conformations consisting of several combinations of C–C or even C=N imine bond isomerizations with a wide range of torsional angles. In a non-polar and less polar solvent medium with a low water content (THF:water = 9:1), this type of molecular conformation is expected to prefer a non-radiative deactivation pathway leading to a minimum luminescence quantum yield for **L1** (2.15%). In contrast, in a polar solvent with an increased percentage of water (THF:water = 1:1) the monomeric building blocks arrange themselves into a well-organized structure with increased luminescence quantum yield (2.50%) and a red-shifted emission maximum. More importantly, this bathochromic shift of the characteristic ICT-based emission maximum with increasing medium polarity, associated with both the AIE and the ACQ process, could originate from a single aggregated state (same ground state structure) or several aggregated states with different packing systems of the **L1** molecular building block.[48] A polar solvent with a greater percentage of water helps the **L1** molecule to self-assemble with specific conformations through appropriately tuned operative non-covalent interactions, including π–π stacking and intermolecular H-bonding. Such a self-assembly process[49] is expected to enforce certain restrictions on intermolecular torsional motion, which promotes a somewhat more planar conformation of the **L1** molecule. This fact may be responsible for the lowering of the excited state energy and redshift of the characteristic ICT-based emission maxima of **L1**. Therefore, our UV-Vis and steady-state fluorescence spectral analysis of **L1** in different solvent media of varying polarity revealed that in highly polar media with a higher percentage of water, conformations of **L1** with enhanced planarity and conjugation were stabilized in their self-assembled state and accounted for the red-shifted white light emission.[50,51]

Morphological variation

The above results indicate that with increasing polarity of the solvent medium, **L1** emits light of multiple colours associated with different self-assembled states of **L1**. We therefore expected the self-assembled **L1**-based structures obtained under varying medium polarity to differ in morphology. For this reason, we triggered the self-assembly of **L1** in THF:water mixtures with a varied percentage of water. In a

THF:water = 7:3 mixture, **L1** self-assembled into thin fibrillar structures that formed a fibrillar network (Fig. 2A and B). In a THF:water = 4:6 mixture, **L1** self-assembled into a fibrillar network consisting of thicker fibrils (Fig. 2C and D). In a highly polar THF:water = 1:9 mixture, **L1** self-assembled into an aggregated network of needle-shaped nanorods (Fig. 2E and F). The emission spectra of **L1** displayed a noticeable red shift of the characteristic emission maximum as the percentage of water in the THF:water mixture increased from 30% to 90% and produced luminescence of different colours ranging from green to yellow and to white (Fig. 2G–I). Fig. 2K shows the formation of different self-assembled superstructures in THF mixed solvents varying in water content. These morphologically varied **L1**-based self-assembled superstructures account for the aggregation-induced multi-colour luminescence described above. Morphological analysis helps to predict the mechanism by which the polarity of the medium induces the aggregation of **L1**. Initially, in a less polar medium (THF:water = 7:3 mixture) **L1** self-assembles into thin fibrils. In a THF:water = 4:6 mixture, **L1** self-assembles into a thicker fibrillar network due to enhanced hydrophobic interactions with increasing water content. When the percentage of water in the THF:water mixture reaches 90%, **L1** self-assembles into needle-shaped nanorods with enhanced dimensions. In a highly polar self-assembly medium with a higher percentage of water, the molecular aggregation process tends to minimize hydrophobic interactions with water as well as the surface energy of self-assembled structures, giving rise to morphological variation in aggregated superstructures in solvents differing in water content (Fig. 2J and K). We carried out our quantitative morphological analysis of the self-assembled superstructures of **L1** obtained in a THF:water mixture of varying polarity based on the distribution of width and length obtained from HR-SEM images (Fig. S4, ESI†). The **L1** fibrils obtained with the THF:water = 7:3 mixture and THF:water = 4:6 mixture were homogeneously distributed, as shown in the SEM images captured at lower magnification. However, the population of fibres varied with the polarity of the self-assembly medium. The length of **L1**-derived fibrils obtained with 7:3 and 4:6 THF:water mixtures had an average length of 272 ± 10.1 μm and 255 ± 8.6 μm, respectively. The average length of the **L1**-based self-assembled needle-shaped nanorods obtained in a THF:water = 1:9 mixture was 174 ± 12.8 μm. In contrast, the width of the **L1**-based self-assembled fibrils and nanorods varied noticeably. The thinner fibrils obtained with a THF:water = 7:3 mixture self-assembly medium had an average diameter of ~216 nm whereas the average diameter of the thicker fibril obtained in an THF:water = 4:6 mixture was ~360 nm.

With **L1**-derived needle-shaped nanorods, the diameter varied in the range of ~2.5 μm. We further performed dynamic light scattering (DLS) analysis of the self-assembled **L1** with various morphologies obtained from different solvent systems of varying polarity (THF:water = 7:3, 4:6, and 1:9) and the results obtained from the DLS analysis is in good agreement with the morphological analysis through SEM (Fig. S5, ESI†).[48]
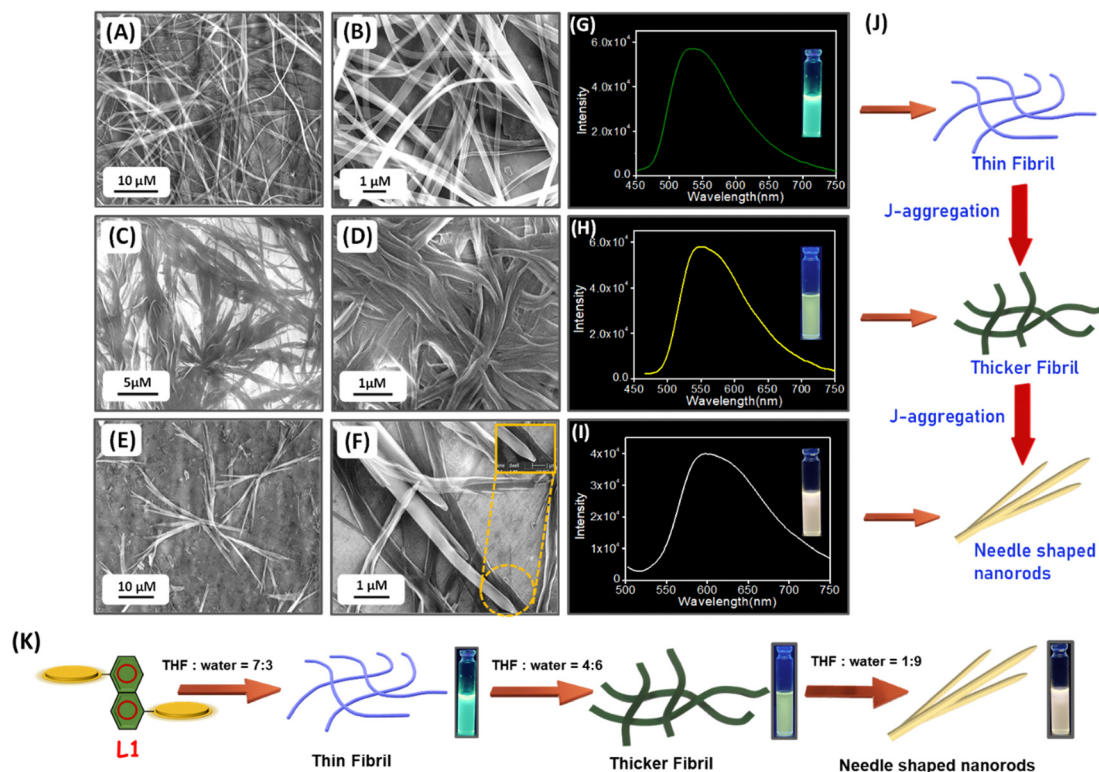
Fig. 2 HR-SEM micrographs of the self-assembled structures formed by **L1** in THF : water = 7 : 3 (A) and (B), THF : water = 4 : 6 (C) and (D) and THF : water = 1 : 9 mixtures (E) and (F). Emission spectra and luminescence colours of self-assembled **L1** were obtained in THF : water = 7 : 3 (G), THF : water = 4 : 6 (H) and THF : water = 1 : 9 mixtures (I). (J) and (K) Pictorical representation of the morphologically different self-assembled structures formed by **L1** building block in THF:water mixtures of varying polarity.

We subsequently aimed to investigate changes in intermolecular non-covalent forces associated with the different self-assembled states of **L1** in different solvent media of varying polarity. In this context, we recorded Fourier transform infrared (FT-IR) spectra **L1** self-assembled in THF : water = 7 : 3 and 1 : 9 medium respectively. The FT-IR spectra of **L1** (solid mass) isolated from a THF : water = 7 : 3 mixture exhibited characteristic peaks at 1602 ($\nu_{C=N(imine)}$), 1493 ($\nu_{C-C(aromatic)}$), 1454 ($\nu_{C-C(aromatic)}$), 1428 ($\nu_{C-N(aromatic)}$), 2884 ($\nu_{C-H(aromatic)}$) and 3213 cm^{-1} ($\nu_{N-H(imidazole)}$). The FT-IR spectra of solid mass obtained with the THF : water = 1 : 9 mixture displayed noticeable changes in the position and intensity of peaks corresponding to $\nu_{C=N(imine)}$, $\nu_{C-C(aromatic)}$, $\nu_{C-N(aromatic)}$, $\nu_{C-C(aromatic)}$ and $\nu_{C-H(aromatic)}$ which unequivocally confirms the varied π–π stacking interactions during the self-assembly of **L1** with changing polarity of the self-assembly medium.[44] On the other hand, a substantial change in the peak position and peak intensity of the characteristic peak corresponding to $\nu_{N-H(imidazole)}$ signifies the further involvement of imidazole (N–H) through intermolecular hydrogen bonding in the molecular self-assembly process of **L1** upon an increase in medium polarity (Fig. 3A and B).[50,52] For further confirmation, we have also recoded the FT-IR spectra of monomeric **L1** (unassembled state, Fig. S6, ESI†). The significant difference in the peak positions and peak intensity of the characteristic peaks compared with the self-assembled sate of **L1** confirmed the

involvement of π–π stacking interaction and intermolecular H-bonding in the self-assembled state.

The modes of molecular aggregation of **L1** in various self-assembled states (obtained by varying the polarity of the self-assembly medium) were investigated further using powder X-ray diffraction (PXRD) analysis of the dried mass of **L1** obtained with the THF : water = 7 : 3 and 1 : 9 mixtures, respectively (Fig. 3C and D). PXRD analysis of the dried mass of **L1** obtained with the THF : water = 7 : 3 mixture revealed diffraction peaks at 19.2 and 24.4° (with d spacing values of 4.6 and 3.6 Å, respectively), which suggests the presence of a π–π stacking interaction between the monomeric building blocks of **L1**. Similar characteristic peaks at 19.4 and 24.5° (with d-spacing values of 4.5 and 3.6 Å) in the PXRD spectrum of dried mass of **L1** obtained from a THF : water = 1 : 9 mixture reflect the existence of intermolecular π–π stacking interactions.[53,54] Furthermore, in the wide-angle region, the diffraction peak appears at 28.5° (with a d-spacing value of 3.1 Å) and 28.3° (with a d-spacing value of 3.1 Å) for the dried mass of **L1** obtained with the THF : water = 7 : 3 and 1 : 9 mixtures, respectively, anticipated in the presence of intermolecular hydrogen bonding involving the imidazole N–H.[53,54] Furthermore, as can be seen from Fig. 3C, diffraction peaks appeared for the thin fibrillar structures self-assembled by **L1** in a THF : water = 7 : 3 mixture at 5.3°, followed by other characteristic nearly periodically spaced peaks at 10.1, 15.9, 21.1 and 26.4° with
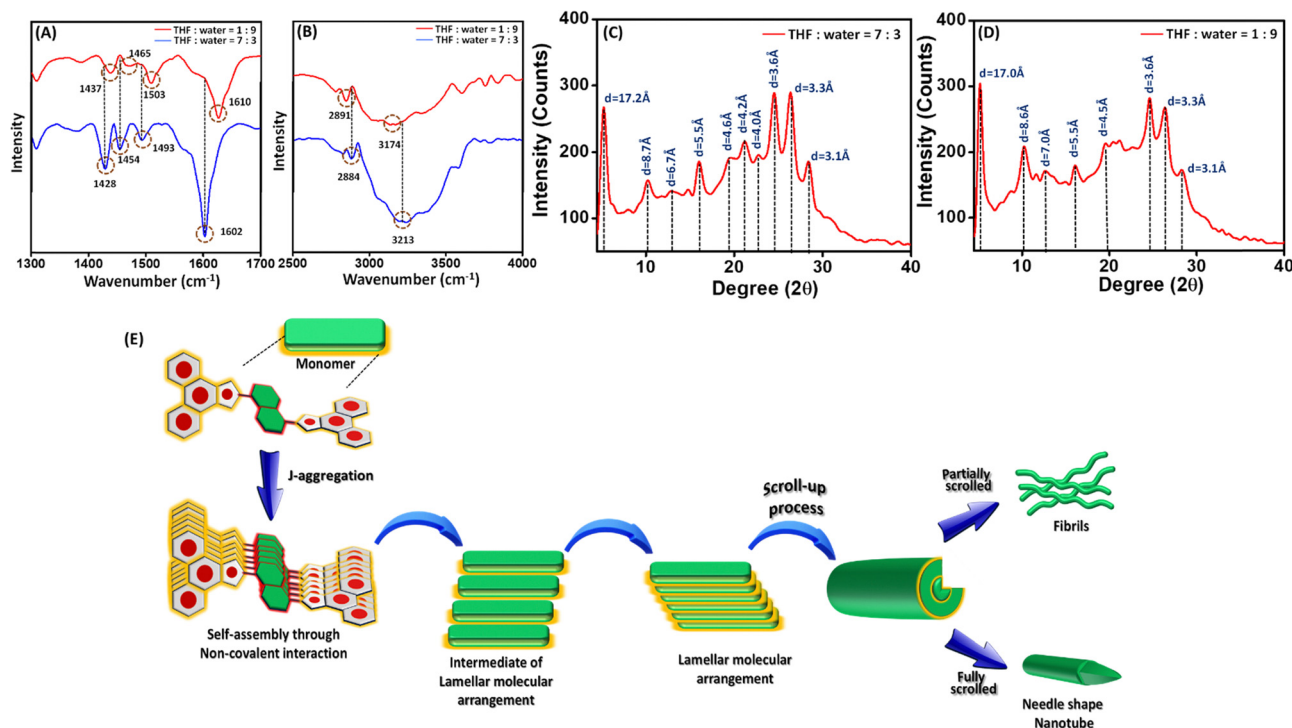
Fig. 3 (A) and (B) FT-IR spectra of the dried mass of **L1** obtained with a THF : water = 7 : 3 mixture (blue) and THF : water = 1 : 9 mixture (red). A PXRD pattern of the dried mass of **L1** obtained with (C) THF : water = 7 : 3 mixture and (D) THF : water = 1 : 9 mixture. (E) Schematic illustration of the formation of fibril- and needle-shaped nanorods by self-assembly of **L1** (via J-aggregation) through intermediate lamellar molecular arrangement followed by layer closure or a scroll-up process in THF:water mixtures with varied polarity.

corresponding d-spacing values of 17.2, 8.7, 5.5, 4.2 and 3.3 Å, respectively. This sequence of ratios approximately equalling 1/2, 1/3, 1/4 and 1/5 suggests that the formation of a lamellar molecular arrangement during the self-assembly of **L1** in the THF : water = 7 : 3 mixture yields thin fibrillar superstructures.[54] The PXRD spectrum of self-assembled **L1** in a highly polar THF : water = 1 : 9 mixture displayed a similar characteristic peak at 5.1° followed by other nearly periodically spaced peaks at 10.2, 16.0, 19.4 and 24.5° with corresponding d-spacing values of 17.0, 8.6, 5.5, 4.5 and 3.6 Å, respectively (Fig. 3D). This periodic ratio is consistent with the lamellar molecular arrangement of **L1** during self-assembly, indicating the formation of tubular superstructures through a layered array of **L1**. To assume an energetically favourable and stable molecular arrangement in a highly polar THF : water = 1 : 9 mixture, the layered lamellar arrangements of **L1** underwent a scroll-up process and generated a superstructure with nanorod-like morphology (Fig. 3E). This scroll-up process not only protects the π-conjugated aromatic moiety from hydrophobic interactions, but also minimizes the surface energy of the resulting superstructures.[53] It is well established that Schiff base compounds are usually unstable in an aqueous medium because of the propensity of the imine bond (C=N) towards hydrolysis in the presence of water. Therefore, there is a possibility that **L1** in an aqueous medium can easily dissociate into its aldehyde (A1) and naphthalene diamine precursors (B1), or its monocondensed intermediate. One detailed ^{1}H NMR study described

the formation of imine molecules from several aldehydes and amines in an aqueous medium within the pH range of 7–11.[55] The study proposed a three-parameter linear equation correlating the logarithms of imine formation constants with pK_a, highest occupied molecular orbital (HOMO) energies of amines, and lowest unoccupied molecular orbital (LUMO) energies of aldehydes, which provide a basis for the search for structural stability correlations conducive to imine formation in an aqueous medium and explain imine formation in such a medium. This result might shed light on different imine formation reactions not only in mixed aqueous media,[56] but also in pure water.[57] It has also been reported that imine-based porous organic cages exhibit comparably excellent hydrolytic stability.[58]

To verify the hydrolytic stability of **L1**, we recorded the UV-Vis absorption and steady-state emission spectra of the precursors imidazole-based aldehyde (A1) and naphthalene diamine (B1) in THF:water mixtures of varying polarity. Noticeable differences in the electronic spectral pattern of the starting aldehyde (A1) and diamine (B1) of **L1** suggest that **L1** is stable in aqueous media (Fig. S7, ESI†). Furthermore, the emission colour of the parental aldehyde (A1) and the diamine (B1) in a THF:water mixture with varied polarity (Fig. S8, ESI†) confirmed that the visually detectable changes in the emission colour of **L1** upon altering the polarity of the medium are due to aggregation induced by changing the medium polarity and not due to hydrolytic decomposition.

DFT studies

To further investigate the proposed self-assembly/aggregation-induced single-molecule fluorescence properties, we performed theoretical geometry optimization and electronic transition calculations for **L1** using density functional theory (DFT) and time-dependent DFT (TDDFT) calculations. The optimized geometry of the **L1** monomer can exist in two different orientations: One, S1, is the open form and the other, S2, is the folded form resulting from intramolecular π–π interactions (Fig. 4a and b). Due to the presence of intramolecular π–π stacking interactions, S2 is more stable, and the energy gap between the S1 and S2 forms decreases with increasing solvent polarity. The dimeric structures, namely the S1 dimer and the S2 dimer, can consist of both monomeric forms S1 and S2, respectively. In our study, we considered two different types of stacking modes: first, in the S1 dimeric form of **L1**, there is tight face-to-face stacking where all aromatic ring planes overlap with the adjacent molecule. Secondly, in contrast, in the S2 dimeric form, π-conjugated phenanthroimidazole-2-yl moieties overlap intermolecularly with each other (Fig. 4c and d). Above we discuss the influence of operative non-covalent interactions and the morphological transformation resulting from changes in molecular assembly patterns associated with varying solvent medium polarity. The first conclusion is that the molecules under consideration are more likely to self-assemble in a highly polar solvent. Secondly, the transformation of the more stable S2 monomer into the S1 monomer is greater with increasing medium polarity. Based on these facts, we can predict the formation of the S2 dimeric form of **L1** in a 100% THF medium whereas the S1 dimeric form of **L1** is preferentially formed in a THF : water = 1 : 9 mixture. The optimized geometries show that the phenanthroimidazole-2-yl moieties in the S1 dimer overlap by approximately 3.528 Å whereas in the S2 dimer this distance increases to 3.648 Å.

To explore the electronic transitions taking place in the π-stacked systems, we performed time-dependent DFT (TDDFT) calculations. The orbitals associated with specific electronic transitions in all compounds considered are elaborated in Fig. 5 and Fig. S9 (ESI†) and Table 1. In the THF medium, the S2 dimer exhibits two transitions at 328.19 nm and 326.46 nm (Table 1). These transitions primarily involve excitations between frontier molecular orbitals, with significant contributions associated with excitations passing from H−2, H−1 and H to L, L+1 and L+3. These transitions mainly involve excitations transferred from phenanthroimidazole-2-yl moieties to the core phenyl group. With a decreasing percentage of THF and increasing percentage of water, the self-assembly of **L1** is enhanced, leading to the formation of an S1 dimeric form of **L1**, which exhibits strong π–π interactions, as observed previously. In a THF : water = 1 : 9 mixture, a bathochromic shift occurs with a transition at 356.66 nm. This red shift of 28–30 nm is in good agreement with our experimental observations. Aggregated dimers in the S1 state of **L1**, stacked in a tightly bound face-to-face arrangement, lower the energy gap between the HOMO and LUMO levels. The transition involves excitations transferred from phenanthroimidazole-2-yl moieties and the LUMO is located on the core phenyl group.

Ab initio molecular dynamics

The π-conjugated molecules self-assemble in polar solvents, and solvent polarity-induced morphological differences of their self-assembled state are responsible for their multi-colour luminescence, which is therefore tuneable. We evaluated the dynamic nature and stability of the π-stacked structure using MD simulations at 300 K over a simulation time of 10 ps. The MD simulation of the S1 dimer in water medium indicates the existence of strong π–π interactions throughout the simulation (Fig. 6). The distance between the centres of mass (COM) of the two S1 monomers does not fluctuate significantly after 4 ps and the monomers are bound together by strong inter-molecular π–π interactions. The π-stacked structure forms hydrogen bonds with explicit water molecules, as shown by the number
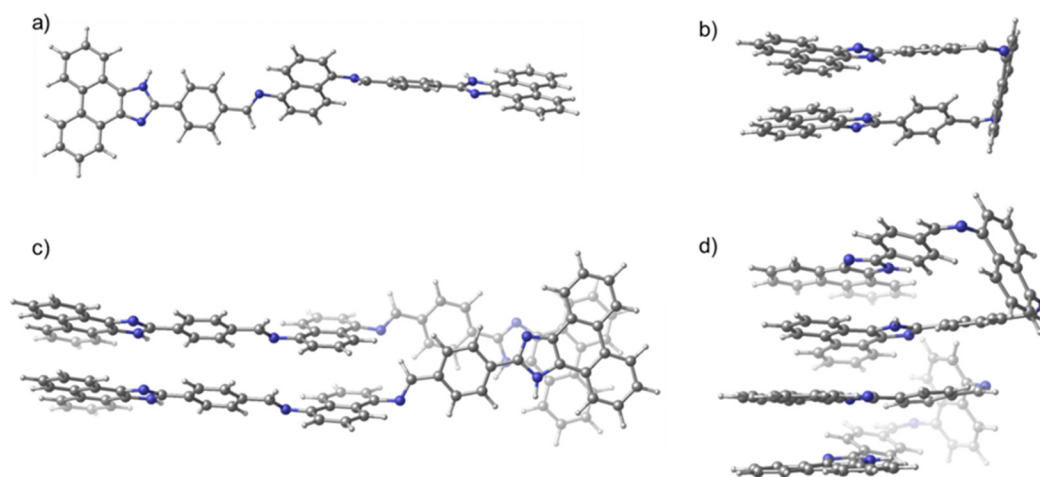

Fig. 4 Optimized geometries of the calculated minima structure of the **L1** monomer are shown in two orientations: (a) open (S1) and (b) stacked (S2). The corresponding dimer is also depicted in two orientations: (c) S1 dimer and (d) S2 dimer. [C: grey, N: blue, H: white].
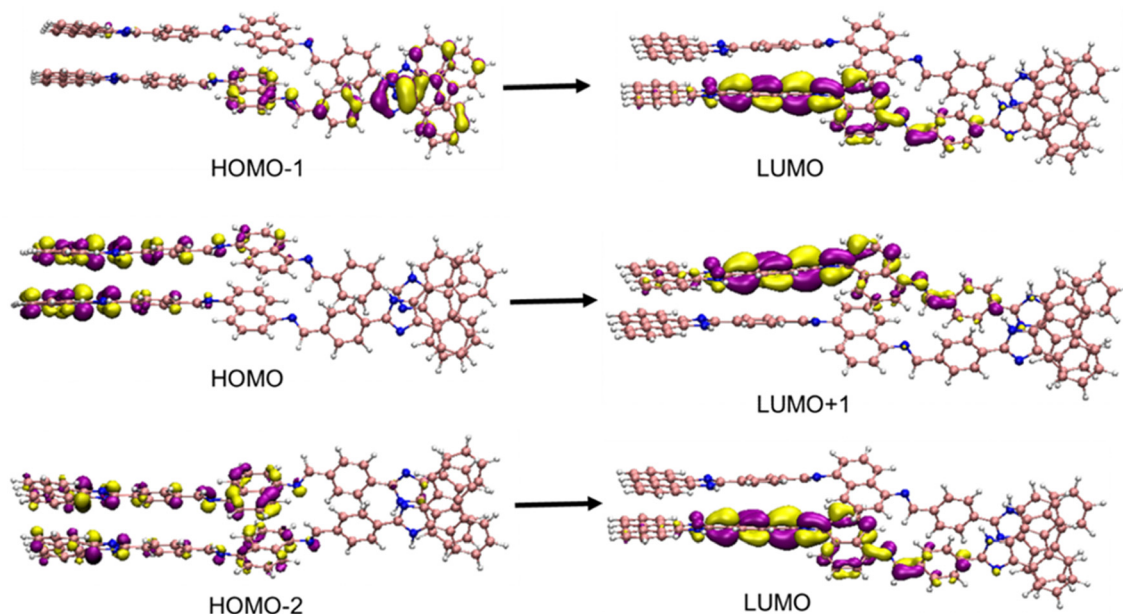
Fig. 5   Frontier molecular orbitals of the calculated minima structure of the **L1** dimer involved in the main absorption peak at wB97XD/def2-TZVPP in a THF : water = 1 : 9 mixture. [C: pink, N: blue, H: white]. The density of the molecular orbitals is shown in yellow and violet with an isosurface value of 0.03.

Table 1   The transition coefficients and associated eigenvalues of the dominated excitation in **L1**

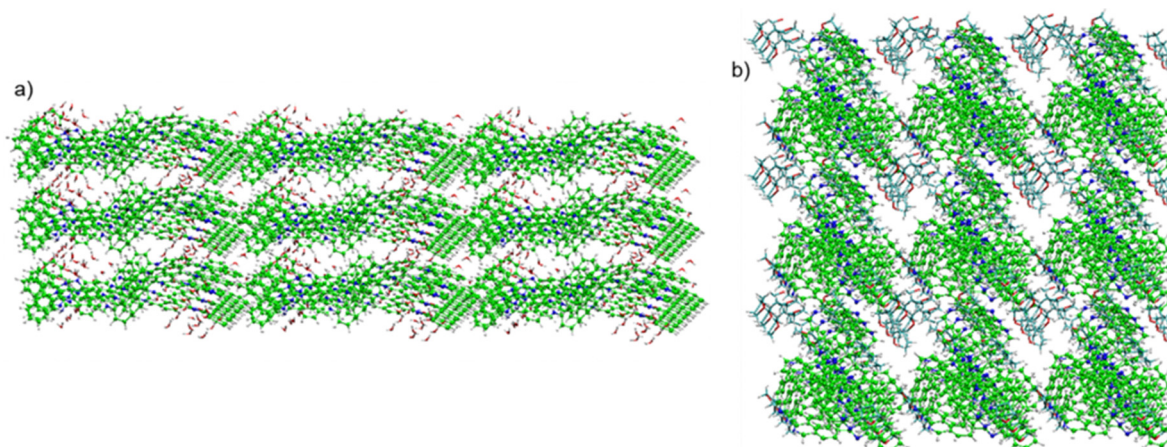|	Medium	Excitation energy (eV)	Wavelength (nm)	Oscillator strength (f)	Key transitions
L1 (S1-dimeric form)	THF : water = 1 : 9	3.476	356.66	4.859	HOMO$-$2 $\rightarrow$ LUMO HOMO$-$1 $\rightarrow$ LUMO HOMO $\rightarrow$ LUMO+1
L1 (S2-dimeric form)	100% THF	3.778	328.19	1.081	HOMO $\rightarrow$ LUMO+3 HOMO$-$2 $\rightarrow$ LUMO HOMO$-$2 $\rightarrow$ LUMO+1
		3.798	326.46	1.002	HOMO $\rightarrow$ LUMO+1 HOMO$-$1 $\rightarrow$ LUMO HOMO$-$1 $\rightarrow$ LUMO+1

Fig. 6   Snapshots taken at a simulation time of 5 ps for (a) the S1 dimeric form of **L1** with water, and (b) the S2 dimeric form of **L1** with THF. [C: green, C(THF): cyan, O: red, H: white].

of hydrogen bonds formed during the simulation time in Fig. S10 (ESI†). However, the S2 dimer does not form significant hydrogen bonds with explicit THF. The distance between the centres of mass (COM) of the two S2 monomers remains large

throughout the simulation time, as illustrated in Fig. S10 (ESI†).

Light-harvesting properties

A mechanistic clarification of this morphological transformation of self-assembled **L1** upon varying the polarity of the self-assembly medium is also expected to inspire questions regarding the potential applications of such self-assembled superstructures with characteristic emission properties. Previously it was described that π-conjugated cyano stilbene derivates are able to self-assemble into a wide range of nanostructures with tuneable emission and transport properties.[59] Gosh *et al.* reported on a supramolecular molecular wire encapsulated into π-conjugated organogels which acts as an efficient light-harvesting antenna with colour-tuneable emission.[60] Intrigued by this finding, we have set out to explore the possibility of using these **L1**-based self-assembled fluorescent superstructures as light-harvesting antenna systems. An efficient Förster resonance energy transfer (FRET) system relies on two critical factors for it to be operational. First, there must be a substantial overlap between the emission spectrum of the donor fluorophore and the absorption spectrum of the acceptor fluorophore. Secondly, the distance between the donor and acceptor fluorophores should ideally be within approximately 10 nm.[59] This spatial closeness allows for efficient energy transfer between these two fluorophores. In this study, to set

up an efficient FRET process, we chose self-assembled **L1**-based superstructures obtained from a THF : water = 1 : 1 mixture as a donor unit and the commercially available fluorescent dye rhodamine B (RhB) as an acceptor unit. RhB exhibits a sharp absorption peak at 560 nm and emits at 580 nm in a THF : water = 1 : 1 mixture (Fig. 7A). On the other hand, **L1** exhibits a broad emission spectrum with an emission maximum at 539 nm (λ_{Ext} = 382 nm) in a THF : water = 1 : 1 mixture (Fig. 7A and B). Noticeable spectral overlap between the emission spectrum of **L1** and the absorption spectrum of RhB suggests that these compounds are an ideal FRET pair for an effective energy transfer process (Fig. 7B). In order to check this, we recorded the emission spectra of three different solutions: (i) self-assembled **L1** (20 μM), (ii) self-assembled **L1** (20 μM) in the presence of RhB (200 nM), and (iii) RhB only (200 nM) in a THF : water = 1 : 1 mixture (λ_{Ext} = 382 nm; Fig. 7B). The emission spectrum recorded for the solution of self-assembled **L1** in the presence of RhB in a THF : water = 1 : 1 mixture produced a strong emission band with an emission maximum at 598 nm (Fig. 7B, red line). In contrast, the spectrum recorded for the solution containing only 20 nM of RhB exhibited insignificant emission (Fig. 7B, pink line). These findings confirm that self-assembling **L1** functions as a light-harvesting antenna and effectively transfers its excitation energy to an RhB acceptor unit. With the gradual addition of greater molar percentages (10–200 nM) of RhB, the emission
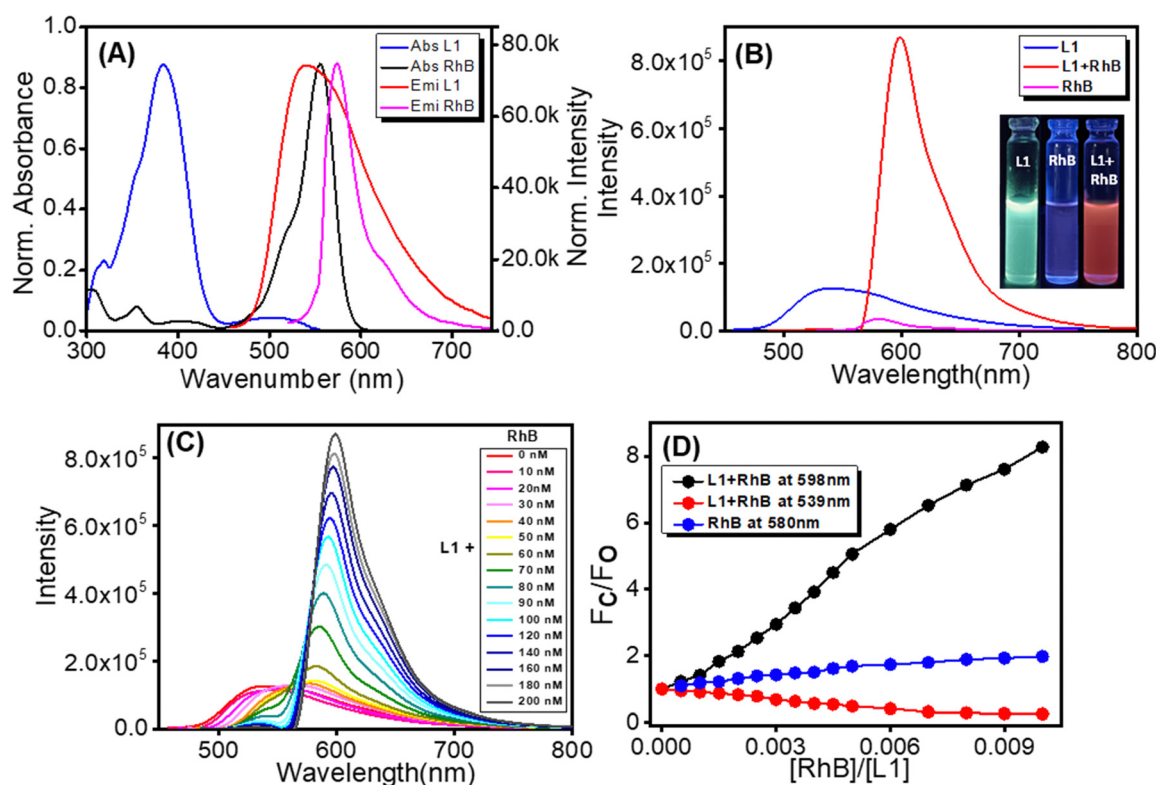

Fig. 7 (A) Absorption spectra of **L1** (blue) and RhB (black) and emission spectra of **L1** (red) and RhB (pink) in the THF : water = 1 : 1 mixture. (B) Emission spectra of **L1** (20 μM, blue), RhB (200 nM, pink) and **L1** (20 μM) + RhB (200 nM) (red; λ_{Ext} = 382 nm); inset: photograph of the emission colour of **L1** (20 μM), RhB (200 nM) and **L1** (20 μM) +RhB (200 nM). (C) Emission spectra of **L1** (20 μM) in the THF : water = 1 : 1 mixture with varying concentrations of RhB. (D) Fluorescence intensity changes at 539 and 598 nm of **L1** + RhB and 580 nm of RhB.

intensity of the self-assembling **L1** is progressively quenched (Fig. 7C). Interestingly, the emission intensity of the RhB increases steadily with a significant redshift of its emission maximum (Fig. 7C). The linear increase of the fluorescence response ratio (F_c/F_0) with increasing concentration of RhB is presented in the inset of Fig. 7D. For further confirmation of this effective energy transfer process, we also recorded the emission spectra of solutions of RhB in varying concentrations from 10 to 200 nM (Fig. 8B). Self-assembled **L1** (the donor) under an increasing concentration of RhB (the acceptor) effectively increases the characteristic emission intensity of RhB (8.2-fold) compared to when it is absent (1.9-fold; see the Fig. 7D). These results clearly demonstrate the efficiency of the energy transfer process between self-assembled **L1** and RhB. The progressive quenching of the characteristic emission of self-assembled **L1** with the gradual addition of

RhB (10 to 200 nM) is due to the effective transfer of excitation energy from self-assembled **L1** to RhB.

Furthermore, we performed time-resolved emission studies to confirm that the energy transfer process outlined above actually takes place. Emission decay profiles of the self-assembled **L1** (λ_{Ext} = 382 nm, λ_{Mon} = 539 nm) and self-assembled **L1** with different amounts of acceptor RhB are presented in Fig. 8A. As the concentration of the acceptor RhB increases from 0 to 200 nM, gradually faster emission decay of self-assembled **L1** is observed along with a drop in calculated average lifetime (τ_{av}) from 4.8 ns to 1.25 ns. This result strongly suggests that effectual energy transfer from self-assembled **L1** to RhB does take place. We have also investigated the energy transfer efficiency (η_{ET}) and the antenna effect (AE) of self-assembled **L1**/RhB systems, as these are crucial parameters for assessing the light-harvesting ability of
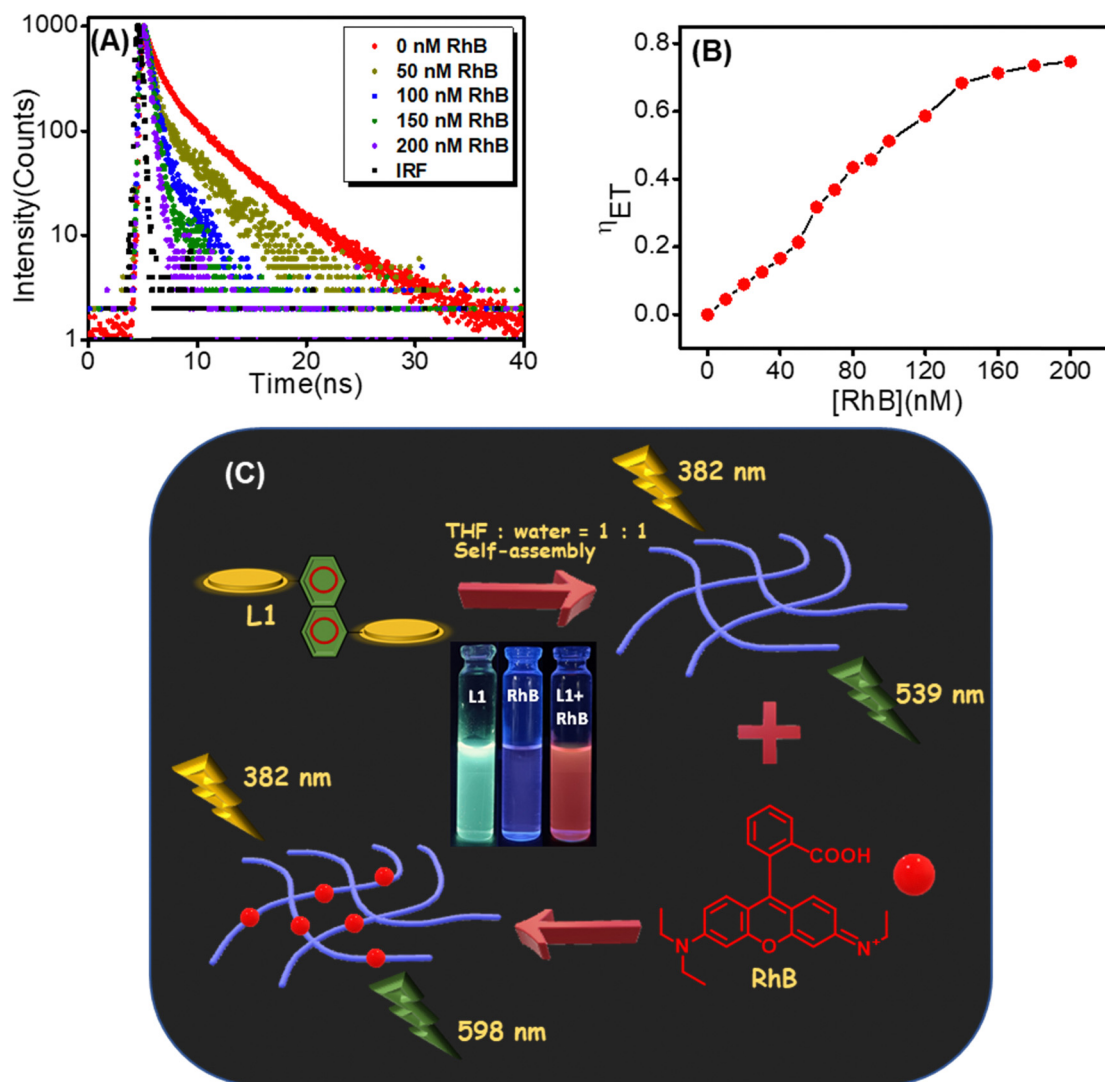

Fig. 8 (A) Fluorescence lifetime decay profiles (λ_{Ext} = 382 nm, monitored at 539 nm) of **L1** upon the addition of different concentrations of RhB (0–200 nM). IRF – instrument response time. (B) Energy transfer efficiency as a function of [RhB]. (C) Schematic representation of the self-assembled **L1**/RhB-based light-harvesting system.

any donor–acceptor system. The efficiency of energy transfer is quantified based on relative changes in emission intensity of self-assembled **L1** as the concentration of RhB increases from 0 to 200 nM (Fig. 8B) using eqn (1).[7,61,62] In the presence of 200 nM of RhB, the energy transfer efficiency reached approximately 74%. The antenna effect (AE) is also quantified by the ratio of emission intensity at the emission maximum of the acceptor in the presence of the donor (λ_{Ext} = 382 nm) (Fig. 7C) to the emission intensity at the emission maximum of the acceptor in the absence of the donor (λ_{Ext} = 560 nm) (Fig. S11, ESI†), formalized by eqn (2).[63] The calculated value of AE for this **L1** (20 μM)/RhB (200 nM)-based donor–acceptor system is 51 (details are given in the ESI† and Table S1),[9] which confirms that this self-assembled **L1**–RhB system is an effective light-harvesting system with a significant antenna effect. Overall, the light-harvesting antenna effect of the donor **L1** and the RhB acceptor is schematically illustrated in Fig. 8C.

$$\eta_{\text{ET}} = 1 - (F_{\text{DA}}/F_{\text{D}}) \qquad (1)$$

$$\text{AE} = F_{\text{A(382nm)}}/F_{\text{A(560nm)}} \qquad (2)$$

Conclusion

We have designed and synthesized a functional small π-conjugated molecule that we call **L1** and explored its optical and self-assembly properties affected by the polarity of the medium in which it self-assembles into higher-level structures. **L1** self-assembles into different superstructures with morphological heterogeneity affected by the polarity of the self-assembly medium, displaying tuneable aggregation-induced fluorescence properties. Therefore, **L1** can be employed for generating multiple fluorescence colours (blue–green–yellow–white) by varying the polarity of the self-assembly medium and, more importantly, can be considered a functional π-conjugated system-based single-component white-light emitter. These significant medium polarity-controlled aggregation-induced emission properties make **L1** a promising candidate for organic electronic and energy transfer applications. We utilized computational analyses, including full geometry optimization, TDDFT calculations and MD simulations, to elucidate the enhanced π–π interaction influenced by solvent polarity and the orbitals involved in the electronic transitions associated with different self-assembled states. Furthermore, we explored the potential applicability of **L1** as a light-harvesting system. Self-assembled superstructures obtained from **L1** in a THF : water = 1 : 1 mixture function as light-harvesting antennae and transfer excitation energy to the commercially available dye rhodamine B with substantial efficiency and an antenna effect. This work not only describes the generation of different superstructures with morphological individualities from a single molecular backbone, but also emphasizes the tuneable aggregation-induced ability of **L1** to emit multi-colour luminescence. It is because of this ability that **L1** might find applications in OLED devices and the fabrication of organic field effect transistors (OFETs). Additionally, the practical applications of

this artificially engineered light-harvesting system can be extended to various other technological domains, including photovoltaics, photocatalysis and photopolymerization. The results of our research therefore potentially significantly contribute to the advancement of materials science and hold substantial promise in the field of organic electronics.

Materials and methods

Materials

All the chemicals and solvents used in the research reported here are commercially available and were used as received without further purification. 9,10-Phenanthrenequinone, naphthalene 1,5-diamine and sodium hydrogen carbonate were purchased from AVRA. Ammonium acetate was purchased from Sisco Research Laboratories (SRL) Pvt. Ltd, India. Glacial acetic acid, acetonitrile and methanol were purchased from Finar Ltd. Terephthaldehyde was purchased from Sigma-Aldrich. Other regular laboratory chemicals were purchased from Sisco Research Laboratory and Loba Chemicals (Mumbai, MH, India).

Synthesis of L1

The detailed protocol utilized to synthesize **L1** is available in the Experimental section of the ESI† (Schemes S1, S2 and Fig. S1–S3, ESI†).

Self-assembly of L1

A fresh stock solution of **L1** was prepared by dissolving this compound in THF to a concentration of 50 mg mL^{-1}. We blended these solutions in several different proportions and diluted them with, THF : water = 7 : 3, THF : water = 4 : 6 and THF : water = 1 : 9 mixtures to achieve the desired concentrations of this building block for self-assembly. The polarized solvent allowed the molecules to self-assemble.

High-resolution scanning electron microscopy (HR-SEM)

A 10 μL drop of a self-assembled solution of **L1** in each of the different solvent media was placed on a glass coverslip and allowed to dry at RT. SEM analysis was performed using a high-resolution scanning electron microscope (HR-SEM, Thermo Scientific Apreo S) operating at 18 kV.

Dynamic light scattering (DLS) analysis

DLS analysis (Zetasizernano ZS, Malvern Instruments, Malvern, UK) was carried out to find the average size distribution of **L1** in THF:water mixtures with varying the solvent polarity.

Fourier transform infrared spectroscopy (FT-IR)

Fourier transform infrared spectra were recorded using an IRTracer-100 FT-IR spectrometer (Shimadzu) with a deuterated lanthanum α-alanine-doped triglycine sulphate (DLaTGS) detector. FT-IR for the dried mass of self-assembled **L1** was carried out in powder form. The measurements were taken at 4 cm^{-1} resolution with an average of 1000 scans. Minimal

transmittance minimal values were determined using the software IR Tracer supplied with the spectrometer.

UV-vis spectroscopy

UV-vis absorption spectra of the synthesized **L1** were recorded in different solvent media with varying polarity using a UV-vis spectrophotometer (Agilent Cary 50 UV-vis double-beam absorption spectrophotometer).

Fluorescence spectroscopy

Fluorescence measurements were performed at RT using a fluorescence spectrophotometer (Edinburgh Instruments, FLS 1000). Emission spectra of the synthesized **L1** were recorded in different solvent media with varying polarity using the appropriate excitation wavelengths.

X-ray diffraction (XRD) analysis

The PXRD pattern of samples was recorded by using a PANalytical X'Pert Pro Powder X-ray diffractometer. Data collection was carried out at room temperature using Cu Kα radiation (1.5406 Å, 40 kV, 30 mA) as the X-ray source in 2θ continuous scan mode (Bragg–Brentano geometry) in the range of 2–50° at a scan rate of 1 scan per minute and a time per step of 0.5 s.

DFT calculations

Monomer geometries were fully optimized using the ωB97XD/def2-TZVPP level whereas those of dimers were optimized at the ωB97XD/def2-SVP level.[64,65] In the solvent, the geometries were optimized with the continuous COSMO solvation model.[66] The solvent was modelled with a dielectric constant of $\varepsilon = 7.4$ (tetrahydrofuran) and $\varepsilon = 76.44$ (10%tetrahydrofuran). All calculations were performed using the Gaussian 16 package.[67]

Time-dependent (TD)-DFT calculations of the complex geometries were performed at the ωB97XD/def2-TZVPP level. The hybrid meta-GGA functional ωB97XD has a 100% fraction of HF exchange at long-range in addition to about 22% at short-range and also contains empirical dispersion terms.[64] Unlike PBE0, the long-range-corrected functional ωB97XD properly describes the ground and excited state properties of complex molecules.[68] The importance of long-range corrected functionals for charged systems and for describing CT states is explained in previous studies.[69,70] The ten lowest vertical excitation energies were calculated based upon time-dependent density functional theory (TDDFT), utilizing optimized geometries.

Periodic boundary condition calculations were performed using the Vienna *Ab initio* Simulation Package (VASP) using the plane-wave basis set.[71,72] All calculations were done on the PBE level of theory using Grimme empirical dispersion.[73] *Ab initio* MD simulations were performed using the isothermal–isobaric (NPT) ensemble until equilibrium was achieved.[74,75] The MD simulation was performed at 300 K using the Langevin thermostat and standard pressure, and the timestep was set to 1 fs.

Author contributions

Priya Rana: analysis and interpretation of data and writing and modification of the manuscript. Mallayasamy Siva: analysis and interpretation of data and writing and modification of the manuscript. Rabindranath Lo: conceptualisation, methodology, and design acquisition of data, analysis and interpretation of data, and writing and editing of the manuscript. Priyadip Das: conceptualisation, methodology, and design acquisition of data, analysis and interpretation of data, writing and editing of the manuscript, study supervision, funding acquisition, and project administration.

Data availability

Characterization data for the compound along with further supporting data referenced in the manuscript are available in the ESI.†

Conflicts of interest

There is no conflict of interest to declare.

Acknowledgements

References

1 G. D. Scholes, G. R. Fleming, A. Olaya-Castro and R. van Grondelle, Lessons from nature about solar light harvesting, *Nat. Chem.*, 2011, **3**, 763–774.

2 R. Croce and H. van Amerongen, Natural strategies for photosynthetic light harvesting, *Nat. Chem. Biol.*, 2014, **10**, 492–501.

3 G. McDermott, S. M. Prince, A. A. Freer, A. M. Hawthornthwaite-Lawless, M. Z. Papiz, R. J. Cogdell and N. W. Isaacs, Crystal structure of an integral membrane light-harvesting complex from photosynthetic bacteria, *Nature*, 1995, **374**, 517–521.

4 Q. Zou, K. Liu, M. Abbas and X. Yan, Peptide-Modulated Self-Assembly of Chromophores toward Biomimetic Light-Harvesting Nanoarchitectonics, *Adv. Mater.*, 2016, **28**, 1031–1043.

5 J. Lalevée, M. Tehfe, F. Dumur, D. Gigmes, B. Graff, F. Morlet-Savary and J. Fouassier, Light-Harvesting Organic

Photoinitiators of Polymerization, *Macromol. Rapid Commun.*, 2013, **34**, 239–245.

6 K. Acharyya, S. Bhattacharyya, H. Sepehrpour, S. Chakraborty, S. Lu, B. Shi, X. Li, P. S. Mukherjee and P. J. Stang, Self-Assembled Fluorescent Pt(II) Metallacycles as Artificial Light-Harvesting Systems, *J. Am. Chem. Soc.*, 2019, **141**, 14565–14569.

7 S. Kundu and A. Patra, Nanoscale Strategies for Light Harvesting, *Chem. Rev.*, 2017, **117**, 712–757.

8 T. Xiao, C. Bao, L. Zhang, K. Diao, D. Ren, C. Wei, Z. Y. Li and X. Q. Sun, An artificial light-harvesting system based on the ESIPT–AIE–FRET triple fluorescence mechanism, *J. Mater. Chem. A*, 2022, **10**, 8528–8534.

9 T. Xiao, D. Ren, L. Tang, Z. Wu, Q. Wang, Z. Y. Li and X. Q. Sun, A temperature-responsive artificial light-harvesting system in water with tunable white-light emission, *J. Mater. Chem. A*, 2023, **11**, 18419–18425.

10 T. Xiao, X. Li, L. Zhang, K. Diao, Z. Y. Li, X. Q. Sun and L. Wang, Artificial stepwise light harvesting system in water constructed by quadruple hydrogen bonding supramolecular polymeric nanoparticles, *Chin. Chem. Lett.*, 2024, **35**, 108618.

11 J. Li, Y. Chen, J. Yu, N. Cheng and Y. Liu, A Supramolecular Artificial Light-Harvesting System with an Ultrahigh Antenna Effect, *Adv. Mater.*, 2017, **29**, 1701905.

12 Z. Zhang, Z. Zhao, Y. Hou, H. Wang, X. Li, G. He and M. Zhang, Aqueous Platinum(II)-Cage-Based Light-Harvesting System for Photocatalytic Cross-Coupling Hydrogen Evolution Reaction, *Angew. Chem., Int. Ed.*, 2019, **58**, 8862–8866.

13 N. Aizawa, C. J. Tsou, I. S. Park and T. Yasuda, Aggregation-induced delayed fluorescence from phenothiazine-containing donor-acceptor molecules for high-efficiency non-doped organic light-emitting diodes, *Polym. J.*, 2017, **49**, 197–202.

14 Y. Li, Y. Dong, L. Cheng, C. Qin, H. Nian, H. Zhang, Y. Yu and L. Cao, Aggregation-Induced Emission and Light-Harvesting Function of Tetraphenylethene-Based Tetracationic Dicyclophane, *J. Am. Chem. Soc.*, 2019, **141**, 8412–8415.

15 A. Arrigo, F. Puntoriero, G. La Ganga, S. Campagna, M. Burian, S. Bernstorff and H. Amenitsch, Aggregation-Induced Energy Transfer in a Decanuclear Os(II)/Ru(II) Polypyridine Light-Harvesting Antenna Dendrimer, *Chem*, 2017, **3**, 494–508.

16 S. Guo, Y. Song, Y. He, X. Hu and L. Wang, Highly Efficient Artificial Light-Harvesting Systems Constructed in Aqueous Solution Based on Supramolecular Self-Assembly, *Angew. Chem.*, 2018, **130**, 3217–3221.

17 P. Chen, Y. Weng, L. Niu, Y. Chen, L. Wu, C. Tung and Q. Yang, Light-Harvesting Systems Based on Organic Nano-crystals To Mimic Chlorosomes, *Angew. Chem., Int. Ed.*, 2016, **55**, 2759–2763.

18 B. Sun, K. Tao, Y. Jia, X. Yan, Q. Zou, E. Gazit and J. Li, Photoactive properties of supramolecular assembled short peptides, *Chem. Soc. Rev.*, 2019, **48**, 4387–4400.

19 J. Lalevée, F. Dumur, C. R. Mayer, D. Gigmes, G. Nasr, M.-A. Tehfe, S. Telitel, F. Morlet-Savary, B. Graff and

J. P. Fouassier, Photopolymerization of N-Vinylcarbazole Using Visible-Light Harvesting Iridium Complexes as Photo-initiators, *Macromolecules*, 2012, **45**, 4134–4141.

20 Z. Zhang, Z. Zhao, Y. Hou, H. Wang, X. Li, G. He and M. Zhang, Aqueous Platinum(II)-Cage-Based Light-Harvesting System for Photocatalytic Cross-Coupling Hydrogen Evolution Reaction, *Angew. Chem.*, 2019, **131**, 8954–8958.

21 J. Yuan, Y. Zhang, J. Yuan, Y. Zhang, L. Zhou, G. Zhang, H. Yip, T. Lau and X. Lu, Single-Junction Organic Solar Cell with over 15% Efficiency Using Fused-Ring Acceptor with Electron-Deficient Core Single-Junction Organic Solar Cell with over 15% Efficiency Using Fused-Ring Acceptor with Electron-Deficient Core, *Joule*, 2017, **3**, 1140–1151.

22 Q. Hongwei, T. Xiao, R. B. P. Elmes and L. Wang, Construction of a sequential light-harvesting system via supramolecular copolymerization, *Chin. Chem. Lett.*, 2023, **34**, 108185.

23 R. T. Gao, S. Y. Li, B. H. Liu, Z. Chen, N. Liu, L. Zhou and Z. Q. Wu, One-pot asymmetric living copolymerization-induced chiral self-assemblies and circularly polarized luminescence, *Chem. Sci.*, 2024, **15**, 2946–2953.

24 N. Liu, R. T. Gao and Z. Q. Wu, Helix-Induced Asymmetric Self-Assembly of π-Conjugated Block Copolymers: From Controlled Syntheses to Distinct Properties, *Acc. Chem. Res.*, 2023, **56**(21), 2954–2967.

25 C. Wang, L. Xu, L. Zhuo, N. Liu and Z. Q. Wu, Asymmetric Living Supramolecular Polymerization: Precise Fabrication of One-Handed Helical Supramolecular Polymers, *Angew. Chem., Int. Ed.*, 2022, **61**, e202207028.

26 Y. X. Li, L. Xu, S. M. Kang, L. Zhou, N. Liu and Z. Q. Wu, Helicity- and Molecular-Weight-Driven Self-Sorting and Assembly of Helical Polymers towards Two-Dimensional Smectic Architectures and Selectively Adhesive Gels, *Angew. Chem., Int. Ed.*, 2021, **60**, 7174–7179.

27 L. Xu, C. Wang, Y. X. Li, X. H. Xu, L. Zhou, N. Liu and Z. Q. Wu, Crystallization-Driven Asymmetric Helical Assembly of Conjugated Block Copolymers and the Aggregation Induced White-light Emission and Circularly Polarized Luminescence, *Angew. Chem., Int. Ed.*, 2020, **59**, 16675–16682.

28 S. Ghosh, B. Jana, A. Ghosh, D. M. Guldi and A. Patra, The Impact of Aggregation of Quaterthiophenes on the Excited State Dynamics, *J. Phys. Chem. Lett.*, 2021, **12**, 3424–3430.

29 X. Yan, P. Zhu and J. Li, Self-assembly and application of diphenylalanine-based nanostructures, *Chem. Soc. Rev.*, 2010, **39**, 1877–1890.

30 A. Maity, F. Ali, H. Agarwalla, B. Anothumakkool and A. Das, Tuning of multiple luminescence outputs and white-light emission from a single gelator molecule through an ESIPT coupled AIEE process, *Chem. Commun.*, 2015, **51**, 2130–2133.

31 T. Singha Mahapatra, H. Singh, A. Maity, A. Dey, S. K. Pramanik, E. Suresh and A. Das, White-light-emitting lanthanide and lanthanide-iridium doped supramolecular gels: modular luminescence and stimuli-responsive behaviour, *J. Mater. Chem. C*, 2018, **6**, 9756–9766.

32 D. Braun, Semiconducting polymer LEDs, *Mater. Today*, 2002, **5**, 32–39.

33 M. Más-Montoya and R. A. J. Janssen, The Effect of H- and J-Aggregation on the Photophysical and Photovoltaic Properties of Small Thiophene-Pyridine-DPP Molecules for Bulk-Heterojunction Solar Cells, *Adv. Funct. Mater.*, 2017, **27**, 1605779.

34 Y.-J. Lee, J. Wang and J. W. P. Hsu, Surface photovoltage characterization of organic photovoltaic devices, *Appl. Phys. Lett.*, 2013, **103**, 173302.

35 X. Gu, E. Zhao, T. Zhao, M. Kang, C. Gui, J. W. Y. Lam, S. Du, M. M. T. Loy and B. Z. Tang, A Mitochondrion-Specific Photoactivatable Fluorescence Turn-On AIE-Based Bioprobe for Localization Super-Resolution Microscope, *Adv. Mater.*, 2016, **28**, 5064–5071.

36 X. Gu, E. Zhao, J. W. Y. Lam, Q. Peng, Y. Xie, Y. Zhang, K. S. Wong, H. H. Y. Sung, I. D. Williams and B. Z. Tang, Mitochondrion-Specific Live-Cell Bioprobe Operated in a Fluorescence Turn-On Manner and a Well-Designed Photoactivatable Mechanism, *Adv. Mater.*, 2015, **27**, 7093–7100.

37 R. Xing, C. Yuan, W. Fan, X. Ren and X. Yan, Biomolecular glass with amino acid and peptide nanoarchitectonics, *Sci. Adv.*, 2023, **9**, eadd8105.

38 J. Chai, Y. Wu, B. Yang and B. Liu, The photochromism, light harvesting and self-assembly activity of a multifunction Schiff-base compound based on the AIE effect, *J. Mater. Chem. C*, 2018, **6**, 4057–4064.

39 P. Rana, G. Marappan, S. Sivagnanam, V. J. Surya, Y. Sivalingam and P. Das, Self-assembly induced tunable multiple fluorescence output from a white light-emitting functionalized single π-conjugated molecule and implication in VOC sensing applications, *Mater. Chem. Front.*, 2022, **6**, 1421–1436.

40 P. Rana, A. Jennifer G, S. Rao T, S. Mukhopadhyay, E. Varathan and P. Das, Polarity-Induced Morphological Transformation with Tunable Optical Output of Terpyridine–Phenanthro[9,10-d]imidazole-Based Ligand and Its Zn(II) Complexes with I – V Characteristics, *ACS Omega*, 2023, **8**, 48855–48872.

41 Y. Okazawa, K. Kondo, M. Akita and M. Yoshizawa, Polyaromatic Nanocapsules Displaying Aggregation-Induced Enhanced Emissions in Water, *J. Am. Chem. Soc.*, 2015, **137**, 98–101.

42 W. Z. Yuan, P. Lu, S. Chen, J. W. Y. Lam, Z. Wang, Y. Liu, H. S. Kwok, Y. Ma and B. Z. Tang, Changing the Behavior of Chromophores from Aggregation-Caused Quenching to Aggregation-Induced Emission: Development of Highly Efficient Light Emitters in the Solid State, *Adv. Mater.*, 2010, **22**, 2159–2163.

43 M. Belletête, J. Bouchard, M. Leclerc and G. Durocher, Photophysics and solvent-induced aggregation of 2,7-carbazole-based conjugated polymers, *Macromolecules*, 2005, **38**, 880–887.

44 J. Luo, Z. Xie, Z. Xie, J. W. Y. Lam, L. Cheng, H. Chen, C. Qiu, H. S. Kwok, X. Zhan, Y. Liu, D. Zhu and B. Z. Tang, Aggregation-induced emission of 1-methyl-1,2,3,4,5-pentaphenylsilole, *Chem. Commun.*, 2001, 1740–1741.

45 H. Piwonski, S. Nozue, H. Fujita, T. Michinobu and S. Habuchi, Organic J-Aggregate Nanodots with Enhanced Light Absorption and Near-Unity Fluorescence Quantum Yield, *Nano Lett.*, 2021, **21**(7), 2840–2847.

46 N. J. Hestand and F. C. Spano, Expanded Theory of H- and J-Molecular Aggregates: The Effects of Vibronic Coupling and Intermolecular Charge Transfer, *Chem. Rev.*, 2018, **118**(15), 7069–7163.

47 S. B. Anantharaman, J. Kohlbrecher, G. Raino, S. Yakunin, T. Stoferle, J. Patel, M. Kovalenko, R. F. Mahrt, F. A. Nuesch and J. Heier, Enhanced Room-Temperature Photoluminescence Quantum Yield in Morphology Controlled J-Aggregates, *Adv. Sci.*, 2021, **8**(4), 1903080.

48 S. Banerjee, A. K. Both and M. Sarkar, Probing the Aggregation and Signaling Behavior of Some Twisted 9,9′-Bianthryl Derivatives: Observation of Aggregation-Induced Blue-Shifted Emission, *ACS Omega*, 2018, **3**(11), 15709–15724.

49 H. Zhang, K. Liu, S. Li, X. Xin, S. Yuan, G. Ma and X. Yan, Self-Assembled Minimalist Multifunctional Theranostic Nanoplatform for Magnetic Resonance Imaging-Guided Tumor Photodynamic Therapy, *ACS Nano*, 2018, **12**, 8266–8276.

50 D. C. Lee, K. Jang, K. K. McGrath, R. Uy, K. A. Robins and D. W. Hatchett, Self-assembling asymmetric bisphenazines with tunable electronic properties, *Chem. Mater.*, 2008, **20**, 3688–3695.

51 L. Zhao, X. Ren and X. Yan, Assembly Induced Super-Large Red-Shifted Absorption: The Burgeoning Field of Organic Near-Infrared Materials, *CCS Chem.*, 2021, **3**, 678–693.

52 C. Zhao, X. Qiao, Z. Yi, Q. Guan and W. Li, Active centre and reactivity descriptor of a green single component imidazole catalyst for acetylene hydrochlorination, *Phys. Chem. Chem. Phys.*, 2020, **22**, 2849–2857.

53 A. Maity, A. Dey, M. Gangopadhyay and A. Das, Water induced morphological transformation of a poly(aryl ether) dendron amphiphile: Helical fibers to nanorods, as light-harvesting antenna systems, *Nanoscale*, 2018, **10**, 1464–1473.

54 A. Arul, P. Rana, K. Das, I. Pan, D. Mandal, A. Stewart, B. Maity, S. Ghosh and P. Das, Fabrication of self-assembled nanostructures for intracellular drug delivery from diphenylalanine analogues with rigid or flexible chemical linkers, *Nanoscale Adv.*, 2021, **3**, 6176–6190.

55 C. Godoy-Alcántar, A. K. Yatsimirsky and J. M. Lehn, Structure-stability correlations for imine formation in aqueous solution, *J. Phys. Org. Chem.*, 2005, **18**, 979–985.

56 V. Goral, M. I. Nelen, A. V. Eliseev and J. M. Lehn, Double-level "orthogonal" dynamic combinatorial libraries on transition metal template, *Proc. Natl. Acad. Sci. U. S. A.*, 2001, **98**, 1347–1352.

57 O. Ramström, S. Lohmann, T. Bunyapaiboonsri and J. Lehn, Dynamic Combinatorial Carbohydrate Libraries: Probing the Binding Site of the Concanavalin A Lectin, *Chem. – A Eur. J.*, 2004, **10**, 1711–1715.

58 T. Hasell, M. Schmidtmann, C. A. Stone, M. W. Smith and A. I. Cooper, Reversible water uptake by a stable imine-based porous organic cage, *Chem. Commun.*, 2012, **48**, 4689.

59 B. K. An, J. Gierschner and S. Y. Park, π-Conjugated Cyanostilbene Derivatives: A Unique Self-Assembly Motif for Molecular Nanostructures with Enhanced Emission and Transport, *Acc. Chem. Res.*, 2012, **45**, 544–554.

60 A. Ajayaghosh, V. K. Praveen, C. Vijayakumar and S. J. George, Molecular Wire Encapsulated into π Organogels: Efficient Supramolecular Light-Harvesting Antennae with Color-Tunable Emission, *Angew. Chem.*, 2007, **119**, 6376–6381.

61 G. Sun, M. Zuo, W. Qian, J. Jiao, X. Y. Hu and L. Wang, Highly efficient artificial light-harvesting systems constructed in aqueous solution for supramolecular photocatalysis, *Green Synth. Catal.*, 2021, **1**, 32–37.

62 T. Tsukamoto, T. Shimada and S. Takagi, Artificial Photosynthesis Model: Photochemical Reaction System with Efficient Light-Harvesting Function on Inorganic Nanosheets, *ACS Omega*, 2018, **13**, 18563–18571.

63 L. Olejko and I. Bald, FRET efficiency and antenna effect in multi-color DNA origami-based light harvesting systems, *RSC Adv.*, 2017, **7**, 23924–23934.

64 J. Chai, M. Head-gordon, J. Chai and M. Head-gordon, Systematic optimization of long-range corrected hybrid density functionals, *J. Chem. Phys.*, 2008, **8**, 084106.

65 M. Alipour and P. Fallahzadeh, First principles optimally tuned range-separated phosphorus – hydrogen spin – spin coupling, *Phys. Chem. Chem. Phys.*, 2016, **18**, 18431–18440.

66 A. Klamt and G. Schuurmann, COSMO: A New Approach to Dielectric Screening in Solvents with Explicit Expressions for the Screening Energy and its Gradient, *J. Chem. Soc., Perkin Trans. 2*, 1993, 799–805.

67 M. J. Frisch, G. W. Trucks, H. B. Schlegel, G. E. Scuseria, M. A. Robb, J. R. Cheeseman, G. Scalmani, V. Barone, G. A. Petersson, H. Nakatsuji, X. Li, M. Caricato, A. V. Marenich, J. Bloino, B. G. Janesko, R. Gomperts, B. Mennucci, H. P. Hratchian, J. V. Ortiz, A. F. Izmaylov, J. L. Sonnenberg, D. Williams-Young, F. Ding, F. Lipparini, F. Egidi, J. Goings, B. Peng, A. Petrone, T. Henderson, D. Ranasinghe, V. G. Zakrzewski, J. Gao, N. Rega, G. Zheng, W. Liang, M. Hada, M. Ehara, K. Toyota, R. Fukuda, J. Hasegawa, M. Ishida, T. Nakajima, Y. Honda, O. Kitao, H. Nakai, T. Vreven, K. Throssell, J. A. Montgomery, Jr., J. E. Peralta, F. Ogliaro, M. J. Bearpark, J. J. Heyd, E. N. Brothers, K. N. Kudin, V. N. Staroverov, T. A. Keith, R. Kobayashi, J. Normand, K. Raghavachari, A. P. Rendell, J. C. Burant, S. S. Iyengar, J. Tomasi, M. Cossi, J. M. Millam, M. Klene, C. Adamo, R. Cammi, J. W. Ochterski, R. L. Martin, K. Morokuma, O. Farkas, J. B. Foresman, and D. J. Fox, *Gaussian 16, Revision C.02*, Gaussian, Inc., Wallingford CT, 2019.

68 Z. Chen, Y. Li, Z. He, Y. Xu and W. Yu, Theoretical investigations on charge transport properties of tetrabenzo [a, d, j, m] coronene derivatives using different density functional and wB97XD), *J. Chem. Res.*, 2019, **43**, 293–303.

69 L. Zhu, C. Yang, Y. Yi and Z. Wei, Effective Modulation of Exciton Binding Energies in Polymorphs of a Small-Molecule Acceptor for Organic Photovoltaics, *J. Phys. Chem. Lett.*, 2020, **11**, 10227–10232.

70 D. A. Links, Lowest excited states and optical absorption spectra of donor–acceptor copolymers for organic photovoltaics: a new picture emerging from tuned long-range corrected density functionals, *Phys. Chem. Chem. Phys.*, 2012, **14**, 14243–14248.

71 G. Kresse and J. Furthmiiller, Efficiency of ab-initio total energy calculations for metals and semiconductors using a plane-wave basis set, *Comput. Mater. Sci.*, 1996, **6**, 15–50.

72 G. Kresse and D. Joubert, From ultrasoft pseudopotentials to the projector augmented-wave method, *Phys. Rev. B: Condens. Matter Mater. Phys.*, 1999, **59**, 11–19.

73 S. Grimme, S. Ehrlich and L. Goerigk, Effect of the Damping Function in Dispersion Corrected Density Functional Theory, *J. Comput. Chem.*, 2011, **38**, 1456–1465.

74 A. R. M. Parrinello, Crystal structure and pair potential: A Molecular-Dynamics study, *Phys. Rev. Lett.*, 1980, **45**, 1196.

75 M. Parrinello and A. Rahman, Polymorphic transitions in single crystals: A new molecular dynamics method, *J. Appl. Phys.*, 1981, **52**, 7182–7190.